

1 Citation: **Hirt, C.**, S.J. Claessens, T. Fecher, M. Kuhn, R. Pail, M. Rexer (2013), New ultra-high
2 resolution picture of Earth's gravity field, *Geophysical Research Letters*, 40(16), 4279-4283, doi:
3 10.1002/grl.50838.

4 5 **New ultra-high resolution picture of Earth's gravity field**

6
7 Christian Hirt^{1*}, Sten Claessens¹, Thomas Fecher², Michael Kuhn¹, Roland Pail², Moritz Rexer^{1,2}

8 ¹ Western Australian Centre for Geodesy, Curtin University, Perth, Australia

9 ² Institute for Astronomical and Physical Geodesy, Technical University Munich, Germany

10 * E-mail: c.hirt@curtin.edu.au

11 12 **Abstract**

13 We provide an unprecedented ultra-high resolution picture of Earth's gravity over all continents
14 and numerous islands within ± 60 degree latitude. This is achieved through augmentation of new
15 satellite and terrestrial gravity with topography data, and use of massive parallel computation
16 techniques, delivering local detail at ~ 200 m spatial resolution. As such, our work is the first-of-
17 its-kind to model gravity at unprecedented fine scales yet with near-global coverage. The new
18 picture of Earth's gravity encompasses a suite of gridded estimates of gravity accelerations,
19 radial and horizontal field components and quasigeoid heights at over 3 billion points covering
20 80% of Earth's land masses. We identify new candidate locations of extreme gravity signals,
21 suggesting that the CODATA standard for peak-to-peak variations in free-fall gravity is too low
22 by about 40%. The new models are beneficial for a wide range of scientific and engineering
23 applications and freely available to the public.

24 25 **Keywords**

26 Earth's gravity field, gravity, quasigeoid, vertical deflections, ultra-high resolution

27 28 **1 Introduction**

29
30 Precise knowledge of the Earth's gravity field structure with high resolution is essential for a
31 range of disciplines, as diverse as exploration and potential field geophysics [*Jakoby and Smilde,*
32 2009], climate and sea level change research [*Rummel, 2012*], surveying and engineering
33 [*Featherstone, 2008*] and inertial navigation [*Grejner-Brzezinska and Wang, 1998*]. While there
34 is a strong scientific interest to model Earth's gravity field with ever-increasing detail, the
35 resolution of today's gravity models remains limited to spatial scales of mostly 2-10 km globally
36 [*Pavlis et al., 2012; Balmino et al., 2012*], which is insufficient for local gravity field
37 applications such as modelling of water flow for hydro-engineering, inertial navigation or in-situ
38 reduction of geophysical gravity field surveys. Up until now, gravity models with sub-km
39 resolution are unavailable for large parts of our planet.

40
41 Here we provide an unprecedented ultra-high resolution view of five components of Earth's
42 gravity field over all continents, coastal zones and numerous islands within ± 60 degree latitude.
43 This is achieved through augmentation of new satellite and terrestrial gravity with topography
44 data [e.g., *Hirt et al. 2010*] and use of massive parallel computation techniques, delivering local
45 detail at 7.2 arc-seconds (~ 200 m in North-South direction) spatial resolution (Section 2). As
46 such, our work is the first-of-its-kind to model gravity at ultra-fine scales yet with near-global

47 coverage. The new picture of Earth's gravity encompasses a suite of gridded estimates of gravity
48 accelerations, radial and horizontal field components and quasigeoid heights at over 3 billion
49 points covering 80% of Earth's land masses and 99.7% of populated areas (Section 3, 4). This
50 considerably extends our current knowledge of the gravity field. The gridded estimates are
51 beneficial for a range of scientific and engineering applications (Section 5) and freely available
52 to the public. Electronic supplementary materials are available providing full detail on the
53 methods applied in this study.

54

55 **2 Data and Methods**

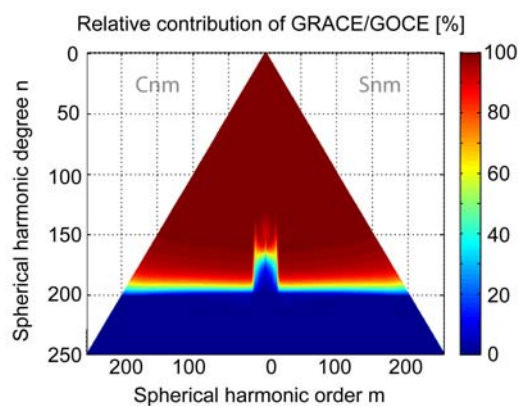
56

57 Our ultra-high resolution picture of Earth's gravity field is a combined solution based on the
58 three key constituents GOCE/GRACE satellite gravity (providing the spatial scales of ~10000
59 down to ~100 km), EGM2008 (~100 to ~10 km) and topographic gravity, i.e., the gravitational
60 effect implied by a high-pass filtered terrain model (scales of ~10 km to ~250 m),
61

62

63 Regarding the satellite component, we use the latest satellite-measured gravity data (release
64 GOCE-TIM4) from the European Space Agency's GOCE satellite [*Drinkwater et al.*, 2003; *Pail*
65 *et al.*, 2011], parameterized as coefficients of a spherical harmonic series expansion, that
66 currently provides the highest-resolution picture of Earth's gravity ever obtained from a space
67 gravity sensor. Resolving gravity field features at spatial scales as short as 80-100 km, GOCE
68 confers new gravity field knowledge, most notably over poorly surveyed regions of Africa,
69 South America and Asia [*Pail et al.*, 2011].

69



70

71 **Figure 1.** Relative contribution of GOCE/GRACE data per spherical harmonic coefficient in the combination with
72 EGM2008 data (in percent) for the degrees 0 to 250

73

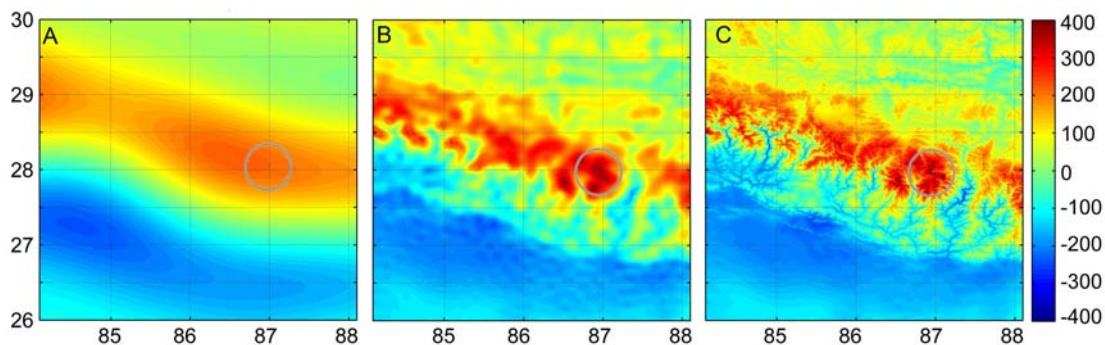
74 Compared to pure GOCE models, complementary GRACE satellite gravity [*Mayer Guerr et al.*,
75 2010] are superior in the spectral range up to degrees 70-80 [*Pail et al.*, 2010]. Therefore, first a
76 combined satellite-only combined solution based on full normal equations of GRACE (up to
77 degree 180) and GOCE (up to degree 250) is computed [see, e.g., *Pail et al.*, 2010]. The
78 GRACE/GOCE combination is then merged with EGM2008 [*Pavlis et al.*, 2012] using the
79 EGM2008 coefficients as pseudo-observations. Since for EGM2008 only the error variances are
80 available, the corresponding normal equations have diagonal structure. In our combination,
81 GRACE/GOCE data have dominant influence in the spectral band of harmonic degrees 0 to 180
82 with EGM2008 information taking over in the spectral range 200 to 2190, leaving the main
83 spectral range of transition from GRACE/GOCE to EGM2008 in spectral band of degrees 181 to

84 200. The relative contributions of EGM2008 and GRACE/GOCE satellite gravity are shown in
85 Fig. 1.

86
87
88

89 The spherical-harmonic coefficients of the combined GRACE/GOCE/EGM2008 (GGE) gravity
90 model were used in the spectral band of degrees 2 to 2190 to synthesize a range of frequently
91 used gravity field functionals at the Earth's surface. For accurate spherical harmonic synthesis at
92 the Earth's surface, as represented through the SRTM topography, the gradient approach to fifth-
93 order [Hirt 2012] was applied. This numerically efficient evaluation technique takes into account
94 the effect of gravity attenuation with height. Applying the gradient approach as described in Hirt
95 [2012] yielded numerical estimates for radial derivatives (gravity disturbances) and horizontal
96 derivatives (deflections of the vertical) of the disturbing potential and quasigeoid heights from
97 the GGE data set at 7.2 arc-sec resolution (about 3 billion surface points) within the SRTM data
98 coverage.

99



100

101 **Figure 2.** Gravity field at different levels of resolution over Mount Everest area. A: satellite-only (free-air) gravity
102 from GOCE and GRACE satellites, B: GGE gravity (satellite gravity combined with EGM2008 gravity), C:
103 GGMplus as composite of satellite gravity, EGM2008 and topographic gravity. Shown is the radial component of
104 the gravity field over a $\sim 400 \times 400$ km area covering parts of the Southern Himalayas including the Mount Everest
105 summit area (marked), units in 10^{-5} m s^{-2} . The spatial resolution of the gravity modelling increases from ~ 100 km
106 (A), ~ 10 km (B) to ultra-fine ~ 200 m spatial scales (C).

107

108 For the Mount Everest region, Fig. 2 exemplifies the associated resolution of GOCE/GRACE
109 satellite gravity (A) and their combination with EGM2008 gravity (B). The spatial resolution of
110 the GGE gravity field functionals is limited to about ~ 10 km (or harmonic degree of 2190) which
111 leaves the problem of modelling the field structures at short scales, down to few 100 m
112 resolution at any of the surface points.

113

114 Because ground gravity measurements at a spatial density commensurate with our model
115 resolution do not exist over most parts of Earth [e.g., Sansò and Sideris, 2013] – and will not
116 become available in the foreseeable future – alternative solutions are required to estimate the
117 gravity field signals at scales shorter than 10 km. High-resolution topography data is widely
118 considered the key to ultra-high resolution gravity modelling and used successfully as effective
119 means to estimate short-scale gravity effects [Sansò and Sideris, 2013; Tziavos and Sideris,
120 2013, Pavlis et al., 2012; Forsberg and Tscherning, 1981]. This is because the short-scale
121 gravity field is dominated by the constituents generated by the visible topographic masses

122 [Forsberg and Tscherning, 1981]. However, forward estimation of the short-scale gravity field
 123 constituents from elevation models near-globally at ultra-high (few 100 metres) resolution is
 124 computationally demanding. Yet we have accomplished this challenge for the first time through
 125 advanced computational resources.

126
 127 Massive parallelization and the use of Western Australia’s iVEC/Epic supercomputing facility
 128 allowed us to convert topography from the Shuttle Radar Topography Mission (SRTM), cf.
 129 *Jarvis et al.* [2008] – along with bathymetric information along coastlines [*Becker et al.*, 2009] –
 130 to topographic gravity at 7.2 arc-sec resolution everywhere on Earth between $\pm 60^\circ$ latitude with
 131 SRTM data available. Based on non-parallelized standard computation techniques, the
 132 calculation of topographic gravity effects would have taken an estimated 20 years, which is why
 133 previous efforts were restricted to regional areas [*Kuhn et al.*, 2009; *Hirt*, 2012].

134
 135 The conversion of topography to topographic gravity is based on the residual terrain modelling
 136 technique [*Forsberg*, 1984], with the topography high-pass filtered through subtraction of a
 137 spherical harmonic reference surface (of degree and order 2160) prior to the forward-modelling.
 138 We treated the ocean water masses and those of the major inland water bodies (Great Lakes,
 139 Baikal, Caspian Sea) using a combination of residual terrain modelling with the concept of rock-
 140 equivalent topography [*Hirt*, 2013], whereby the water masses were ‘compressed’ to layers
 141 equivalent to topographic rock. These procedures yield short-scale topographic gravity that is
 142 suitable for augmentation of degree-2190 spherical harmonic gravity models beyond their
 143 associated 10 km resolution, cf. *Hirt* [2010; 2013]. The topographic gravity is based on a mass-
 144 density assumption of 2670 kg m^{-3} and provides the spatial scales of $\sim 10 \text{ km}$ to $\sim 250 \text{ m}$, which is
 145 complementary to the GGE gravity (spatial scales from $\sim 10000 \text{ km}$ to $\sim 10 \text{ km}$).

146 147 **3 Results**

148
 149 Addition of both components (GGE and topographic gravity) result in the ultra-high resolution
 150 model GGMplus (Global Gravity Model, with plus indicating the leap in resolution over
 151 previous 10 km resolution global gravity models). The modelled gravity field components and
 152 their descriptive statistics are reported in Table 1.

153
 154 **Table 1.** Descriptive statistics of the GGMplus model components calculated at 3,062,677,383 land and
 155 near-coastal points within $\pm 60^\circ$ geographic latitude. RMS is the root-mean-square of the component.

Gravity model component		Min	Max	RMS	Unit
Gravity	Free-fall acceleration	976392	981974	980133	10^{-5} m s^{-2}
	Radial component	-456	714	48.0	10^{-5} m s^{-2}
Horizontal components	North-South	-108	94	6.9	arc-sec
	East-West	-83	79	6.8	arc-sec
	Total (magnitude)	0	109	9.4	arc-sec
Quasigeoid		-99.26	86.60	29.91	m

156
 157 This world-first ultra-high resolution modelling over most of Earth’s land areas delivered us the
 158 expected gravity signatures of small-scale topographic features – such as mountain peaks and
 159 valleys – which are otherwise masked in 10 km resolution models. This adds much local detail to
 160 the gravity maps (compare Figs. 2B and 2C) and yields a spectrally more complete and accurate
 161 description of the gravity field [e.g., *Hirt*, 2012].

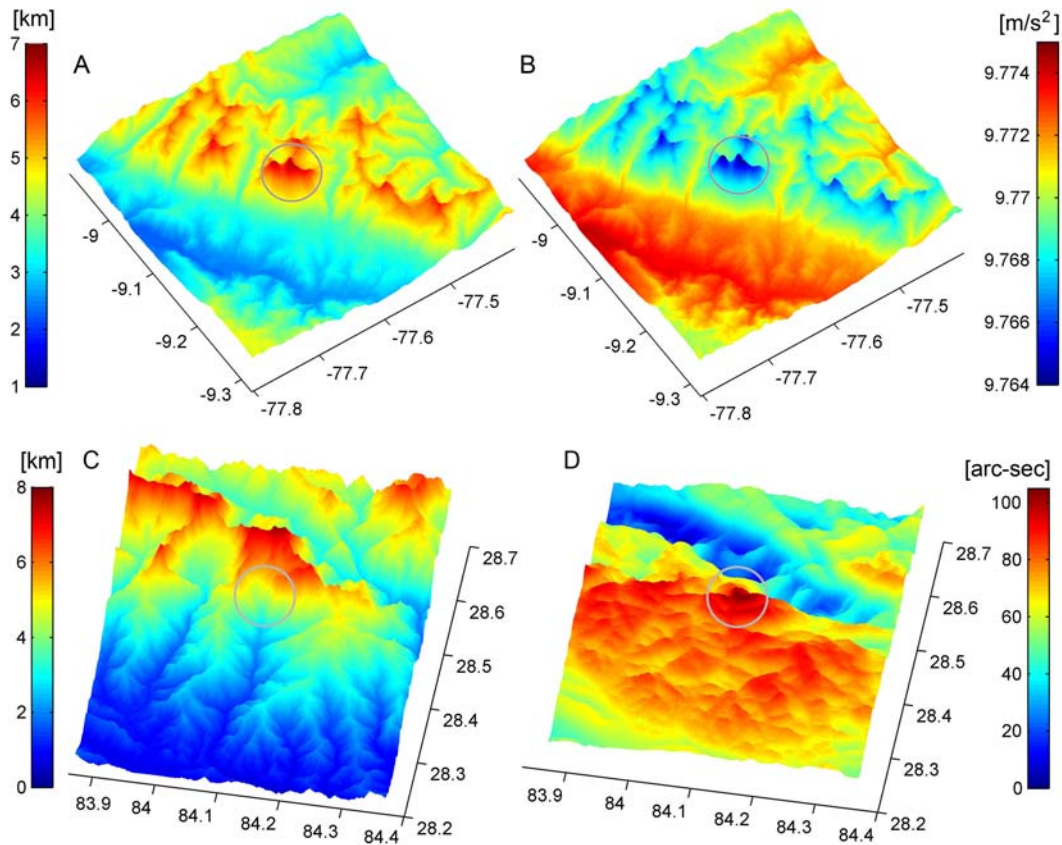
162 **Table 2.** Candidate locations for extreme values of Earth's gravity field

Gravity component	Minimum/ Maximum	Latitude/ Longitude	Geographic feature/ location
Gravity acceleration	9.76392 m s ⁻² 9.83366 m s ⁻²	-9.12°/ -77.60° 86.71°/61.29°	Huascarán, Peru *Arctic Sea
Radial component	-456 × 10 ⁻⁵ m s ⁻² 714 × 10 ⁻⁵ m s ⁻²	29.71°/95.36° 10.83°/-73.69°	Gandengxiang, China Pico Cristóbal Colón, Columbia
Horizontal component ⁺	109 arc-sec	28.45°/84.13°	~10 km South of Annapurna II, Nepal
Quasigeoid	-106.59 m 86.60 m	4.71°/78.79° -8.40°/147.35°	*Laccadive Sea, South of Sri Lanka Puncak Trikora, Papua, Indonesia

163 * offshore area, value estimated without topographic gravity using GGE-only (10 km resolution, also see
164 electronic supplement)

165 ⁺ total component computed as magnitude from the North-South and East-West components

166



167 **Figure 3.** Candidate locations of some extreme signals in Earth's gravity in the Andes (A,B) and Himalaya regions
168 (C,D). Top: Topography (A) and free-fall gravity accelerations (B) over the Huascarán region (Peru), where
169 GGMplus gravity accelerations are as small as ~9.764 m s⁻² (B). Bottom: Topography (C) and GGMplus total
170 horizontal field component (D) over the Annapurna II region (Nepal). The gravitational attraction of the Annapurna
171 II masses is expected to cause an extreme slope of the quasi/geoid with respect to the Earth ellipsoid of up to ~109
172 arc-seconds (D).
173

174 Our gridded estimates portray the subtle variations of gravity (Fig. 3) which are known to depend
175 on factors such as location, height and presence of mass-density anomalies. GGMplus reveals a
176 candidate location for the minimum gravity acceleration on Earth: the Nevado Huascarán summit
177 (Peru) with an estimated acceleration of 9.76392 m s^{-2} (Fig 3A, 3B, and Table 2). A candidate
178 location for Earth's maximum gravity acceleration was identified - outside the SRTM area, based
179 on GGE-only - in the Arctic sea with an estimated 9.83366 m s^{-2} . This suggests a variation range
180 (peak-to-peak variation) for gravity accelerations on Earth of about $\sim 0.07 \text{ m s}^{-2}$, or 0.7 %, which
181 is about 40 % larger than the variation range of 0.5 % implied by standard models based on a
182 rotating mass-ellipsoid (gravity accelerations are 9.7803 m s^{-2} (equator) 9.8322 m s^{-2} (poles) on
183 the mass-ellipsoid, cf. *Moritz* [2000]). So far such a simplified model is also used by the
184 Committee on Data for Science and Technology (CODATA) to estimate the variation range in
185 free-fall acceleration on Earth [*Mohr and Taylor*, 2005]. However, due to the inhomogeneous
186 structure of Earth, presence of topographic masses, and decay of gravity with height the actual
187 variations in free-fall accelerations are $\sim 40\%$ larger at the Earth's surface (Table 2).

188
189 GGMplus free-air gravity - the radial component of Earth's gravity field - varies within a range
190 of $\sim 0.011 \text{ m s}^{-2}$ ($\sim 0.1\%$ of gravity accelerations) with its minimum value of $-456 \times 10^{-5} \text{ m s}^{-2}$
191 located in China and its maximum of $714 \times 10^{-5} \text{ m s}^{-2}$ expected for the Pico Cristóbal Colón
192 summit in Colombia. The higher variability of gravity accelerations over free-air gravity reflects
193 the well-known fact that gravity accelerations include the gravitational attraction and centrifugal
194 effect due to Earth rotation.

195
196 The horizontal components of the gravitational field describe in approximation the North-South
197 and East-West inclination of the quasi/geoid with respect to the reference ellipsoid. The variation
198 range of the horizontal field components (also known as deflections of the vertical) is about ~ 200
199 arc-seconds in North South, and ~ 160 arc-seconds in East-West, respectively (Table 1).
200 GGMplus reveals a candidate location for Earth's largest deflection of the vertical: about 10 km
201 South of Annapurna II, Nepal, the plumb line is expected to deviate from the ellipsoid normal by
202 an angle as large as ~ 109 arc-seconds (Fig. 3C and 3D). This translates into a most extreme
203 quasi/geoid slope of about 0.5 m over 1 km.

204 205 **4 Model evaluation**

206
207 We have comprehensively compared GGMplus gravity field maps with in-situ (direct)
208 observations of Earth's gravity field from gravimetry, astronomy, and surveying (see electronic
209 supplementary materials). Over well-surveyed areas of North America, Europe and Australia,
210 the comparisons suggest an accuracy level for free-air gravity and gravity accelerations of $\sim 5 \times$
211 10^{-5} m s^{-2} , for horizontal field components of about 1 arc-second, and for quasigeoid heights of
212 0.1 m or better.

213
214 Despite the improvements conferred by recent satellite gravity to our model, the GGMplus
215 accuracy deteriorates by a factor of ~ 3 to ~ 5 over Asia, Africa and South America which are
216 regions with limited or very limited ground gravity data availability. Comparisons suggest a
217 decrease in accuracy down to $\sim 20 \times 10^{-5} \text{ m s}^{-2}$ for gravity, ~ 5 arc-seconds for horizontal field
218 components, and $\sim 0.3 \text{ m}$ for quasigeoid heights. The reduced accuracy estimates mainly reflect
219 the limited availability of gravity observations at spatial scales of ~ 100 to $\sim 10 \text{ km}$. The accuracy

220 of GGMplus gravity accelerations will always be lower than that of free-air gravity. This is
221 because accelerations are directly affected by errors in the elevation data, with an elevation error
222 of 10 m equivalent to about $3 \times 10^{-5} \text{ m s}^{-2}$.

223
224 Given that any gravity field signals originating from local mass-density variations are not
225 represented by the topographic gravity, our gravity maps cannot provide information on
226 geological units at scales less than 10 km. This is akin to EGM2008 at spatial scales of ~30 to
227 ~10 km over many land areas where gravity measurements are unavailable or of proprietary
228 nature [Pavlis *et al.*, 2012]. Any global, regional or local gravity map or quasi/geoid model can
229 only be geologically interpreted down to a resolution commensurate with the gravity
230 observations used to construct the model. Nevertheless, incorporation of topographic gravity to
231 approximate gravity field features at spatial scales of ~10 km to ~250 m significantly improves
232 GGMplus gravity and horizontal components when compared to 10 km-resolution maps.
233 Depending on the terrain ruggedness, the observed improvement rates mostly range between 40
234 to 90% for radial and horizontal field components (Supplementary Tables 6 and 8), while the
235 quasigeoid improvement is best observable over rugged areas (up to 40 % improvement,
236 Supplementary Table 9).

237
238 **5 Applications**
239 Apart from enhancing our knowledge of Earth's gravity and its variations, there are several
240 scientific and engineering applications that require high-resolution and largely complete gravity
241 knowledge, which is now available through GGMplus gravity maps.

242
243 The quasi/geoid plays a crucial role in modern determination of topographic heights with Global
244 Navigation Satellite Systems (such as the Global Positioning System GPS), allowing the
245 measurement of heights above mean sea level rather than heights above the ellipsoid [e.g., Meyer
246 *et al.*, 2006; Featherstone, 2008; Hirt *et al.*, 2011]. While several regional-size quasi/geoid
247 models of good quality are available at mostly ~2 km resolution over well-surveyed land areas
248 (e.g., Europe, USA, Australia), GGMplus is capable of providing improved quasi/geoid
249 information over those parts of Asia, Africa and South America, where no other source of high-
250 resolution gravity (e.g., from airborne gravity) is available. The GGMplus quasigeoid can be
251 suitable for water flow modelling (e.g., as required in hydro-engineering), and height transfer
252 with satellite systems, and can be of utility for the determination of offsets among continental
253 height systems (e.g., Australia and Europe) and their unification [e.g., Flury and Rummel, 2005;
254 Rummel, 2012]. This in turn will allow for a more consistent comparison of sea level
255 observations at tide gauges across the oceans. Because of incorporation of newer GOCE and
256 GRACE satellite gravity, the GGMplus quasigeoid confers improvements at ~100 km spatial
257 scales over parts of Asia, South America and Africa, while consideration of short-scale
258 quasigeoid effects from topography data improves the resolution of quasigeoid heights over
259 rugged terrain [Hirt *et al.*, 2010].

260
261 GGMplus gravity accelerations and free-air gravity are a promising data source for screening and
262 outlier-detection of terrestrial gravity databases and aid in planning of local precision gravimetric
263 surveys. Gravity accelerations as provided by our maps are required e.g., as a correction in the
264 context of geodetic height systems [e.g., Meyer *et al.*, 2006], for accurate topographic mapping,
265 in metrology for calibration of precision scales [Torge, 1989] and seismometers, and in

266 observational astronomy for meteorological corrections [Corbard *et al.*, 2013]. For geophysics
267 and the exploration industry, GGMplus may prove beneficial as novel data source for in-situ
268 reduction of detailed gravimetric surveys, revealing locations of interest for mineral prospectivity
269 without the need to calculate and apply further rather time-consuming reductions [Jakoby and
270 Smilde, 2009] Finally, horizontal field components are required to correct the impact of the
271 Earth's irregular gravity field, e.g., for inertial navigation at or near the Earth's surface [Grejner-
272 Brzezinska and Wang, 1998], or in the context of civil engineering (e.g., precision surveys for
273 tunnel alignment), Featherstone and Rieger [2000]. All of these applications require spectrally
274 most complete information on the gravity field.

275

276 **6 Conclusions**

277

278 GGMplus provides the most complete description of Earth's gravity at ultra-high resolution and
279 near-global coverage to date. This confers immediate benefits to many applications in
280 engineering, exploration, astronomy, surveying, and potential field geophysics. While GGMplus
281 provides moderate additional information (because of the ultra-high resolution short-scale
282 modelling) over areas with dense coverage of gravity stations (e.g., North America, Europe,
283 Australia), significant improvements are provided over areas with sparse ground gravity
284 coverage (e.g., Asia, Africa, South America). For the latter regions, GGMplus provides for the
285 first time a complete coverage with gravity at ultra-high spatial resolution, thus providing
286 scientific aid to many developing countries. In addition, GGMplus provides crucial information
287 to revise current standards for the maximum range of free-fall gravity accelerations over the
288 Earth's surface. The computerized GGMplus gravity field maps are freely available for science,
289 education and industry via [and http://ddfe.curtin.edu.au/gravitymodels/GGMplus](http://ddfe.curtin.edu.au/gravitymodels/GGMplus).

290

291 **Acknowledgements** We are grateful to the Australian Research Council for funding
292 (DP120102441). This work was made feasible through using advanced computational resources
293 of the iVEC/Epic supercomputing facility (Perth, Western Australia). We thank all developers
294 and providers of data used in this study. Full methods, and detailed evaluation results are
295 available in the electronic supplementary information, and information on data access via the
296 project's website <http://geodesy.curtin.edu.au/research/models/GGMplus>.

297

298 **References**

- 299 Balmino, G., N. Vales, S. Bonvalot and A. Briais (2012), Spherical harmonic modelling to ultra-high degree of
300 Bouguer and isostatic anomalies, *J. Geod.*, 86(7), 499-520, doi: 10.1007/s00190-011-0533-4.
- 301 Becker, J.J., D.T. Sandwell, W.H.F. Smith, J. Braud, B. Binder, J. Depner, D. Fabre, J. Factor, S. Ingalls, S-H. Kim,
302 R. Ladner, K. Marks, S. Nelson, A. Pharaoh, R. Trimmer, J. Von Rosenberg, G. Wallace and P. Weatherall
303 (2009), Global Bathymetry and Elevation Data at 30 Arc Seconds Resolution: SRTM30_PLUS, *Marine*
304 *Geod.*, 32(4), 355-371.
- 305 Corbard T., F. Morand, F. Laclarex, R. Ikhlef, and M. Meftah (2013), On the importance of astronomical refraction
306 for modern Solar astrometric measurements, *Astr. Astrophys.*, April 2, 2013.
- 307 Drinkwater, M.R., R. Floberghagen, R. Haagmans, D. Muzi, and A. Popescu (2003), GOCE: ESA's first Earth
308 Explorer Core mission, In (eds. Beutler, G.B., M.R. Drinkwater, R. Rummel, and R. von Steiger), Earth
309 Gravity Field from Space - from Sensors to Earth Sciences. In the Space Sciences Series of ISSI, Vol. 18,
310 419-432, *Kluwer Academic Publishers*, Dordrecht, Netherlands ISBN: 1-4020-1408-2.
- 311 Featherstone W.E. (2008), GNSS-based heighting in Australia: current, emerging and future issues, *J. Spat. Sci.* 53,
312 115-133.
- 313 Featherstone W.E., and J.M. Rieger (2000), The importance of using deviations of the vertical for the reduction of
314 survey data to a geocentric datum, *Australian Surveyor*, 45, 46-61.

315 Flury, J., and R. Rummel (2006), Future satellite gravimetry for geodesy, *Earth Moon Plan.* 94, 13-29.
316 doi:10.1007/s11038-005-3756-7

317 Forsberg R., and C.C. Tscherning (1981), The use of height data in gravity field approximation by collocation, *J.*
318 *Geophys. Res.*, 86(B9), 7843-7854.

319 Forsberg, R. (1984), A study of terrain reductions, density anomalies and geophysical inversion methods in gravity
320 field modelling, Report 355, *Department of Geodetic Science and Surveying*, Ohio State University,
321 Columbus.

322 Grejner-Brzezinska, D.A., and J. Wang (1998), Gravity modeling for high-accuracy GPS/INS integration,
323 *Navigation*, 45, 3, 209-220.

324 Hirt, C. (2010), Prediction of vertical deflections from high-degree spherical harmonic synthesis and residual terrain
325 model data, *J. Geod.*, 84 (3), 179-190. doi:10.1007/s00190-009-0354-x

326 Hirt, C., W.E. Featherstone and U. Marti (2010), Combining EGM2008 and SRTM/DTM2006.0 residual terrain
327 model data to improve quasigeoid computations in mountainous areas devoid of gravity data, *J. Geod.*, 84(9):
328 557-567, DOI: 10.1007/s00190-010-0395-1..

329 Hirt C., Schmitz M., Feldmann-Westendorff U., Wübbena G., Jahn C.-H., and Seeber G. (2011), Mutual validation
330 of GNSS height measurements from high-precision geometric-astronomical levelling, *GPS Solutions*, 15(2),
331 149-159, DOI 10.1007/s10291-010-0179-3.

332 Hirt, C. (2012), Efficient and accurate high-degree spherical harmonic synthesis of gravity field functionals at the
333 Earth's surface using the gradient approach, *J. Geod.*, 86(9), 729-744, doi: 10.1007/s00190-012-0550-y.

334 Hirt, C. (2013), RTM gravity forward-modeling using topography/bathymetry data to improve high-degree global
335 geopotential models in the coastal zone, *Marine Geod.*, 36(2):1-20, doi:10.1080/01490419.2013.779334.

336 Jacoby, W., and P.L. Smilde (2009), *Gravity interpretation*, Springer, Berlin, Heidelberg.

337 Jarvis, A., H.I. Reuter, A. Nelson, and E. Guevara (2008), Hole-filled SRTM for the globe Version 4, *Available from*
338 *the CGIAR-SXI SRTM 90m database*. Available at: <http://srtm.csi.cgiar.org>.

339 Kuhn, M., W.E. Featherstone, and J.F. Kirby (2009), Complete spherical Bouguer gravity anomalies over Australia,
340 *Australian J. Earth Sci.*, 56, 213-223.

341 Mohr P. J., and B.N. Taylor (2005), CODATA recommended values of the fundamental physical constants: 2002,
342 *Rev. Mod. Phys.* 77 (Jan 2005).

343 Moritz, H. (2000), Geodetic Reference System 1980. *J. Geod.*, 74, 128-140.

344 Meyer T.H., D.R. Roman, and D.B. Zilkoski (2006), What Does Height Really Mean? Part IV: GPS Heighting.
345 *Surveying Land Inf. Sci.* 66, 165-183.

346 Mayer-Gürr, T., E. Kurtenbach, and A. Eicker (2010), ITG-Grace2010 Gravity Field Model. URL:
347 <http://www.igg.uni-bonn.de/apmg/index.php?id=itg-grace2010>, 2010.

348 Pail, R., Goiginger, H., W.-D. Schuh, E. Höck, J.M. Brockmann, T. Fecher, T. Gruber, T. Mayer-Gürr, J. Kusche, A.
349 Jäggi, and D. Rieser (2010), Combined satellite gravity field model GOCO01S derived from GOCE and
350 GRACE, *Geophys. Res. Lett.* 37, L20314, doi: 10.1029/2010GL044906.

351 Pail, R., S. Bruinsma, F. Migliaccio, C. Förste, H. Goiginger, W.-D. Schuh, E. Höck, M. Reguzzoni, J.M.
352 Brockmann, O. Abrikosov, M. Veicherts, T. Fecher, R. Mayrhofer, I. Krasbutter, F. Sansò, and C.C.
353 Tscherning (2011), First GOCE gravity field models derived by three different approaches, *J Geod.*, 85(11),
354 819-843, doi: 10.1007/s00190-011-0467-x.

355 Pavlis N.K., S.A. Holmes, S.C. Kenyon, and J.K. Factor (2012), The development and evaluation of the Earth
356 Gravitational Model 2008 (EGM2008), *J. Geophys. Res.*, 117, B04406, doi:10.1029/2011JB008916.

357 Rummel, R. (2012), Height unification using GOCE. *J. Geod. Sci.* 2, 355-362.

358 Sansò F., and M.G. Sideris (2013), The Local Modelling of the Gravity Field: The Terrain Effects. *Lecture Notes in*
359 *Earth System Sciences* 110, 169, Springer, Berlin Heidelberg.

360 Tziavos, I.N., and M.G. Sideris (2013), Topographic Reductions in Gravity and Geoid Modeling. *Lecture Notes in*
361 *Earth System Sciences* 110, 337-400, Springer, Berlin Heidelberg.

362 Torge W. (1989), *Gravimetry*, de Gruyter, Berlin, New York.

363
364
365
366
367
368
369
370

New ultra-high resolution picture of Earth's gravity field

Christian Hirt^{1*}, Sten Claessens¹, Thomas Fecher², Michael Kuhn¹, Roland Pail², Moritz Rexer^{1,2}

¹ Western Australian Centre for Geodesy, Curtin University, Perth, Australia

² Institute for Astronomical and Physical Geodesy, Technical University Munich, Germany

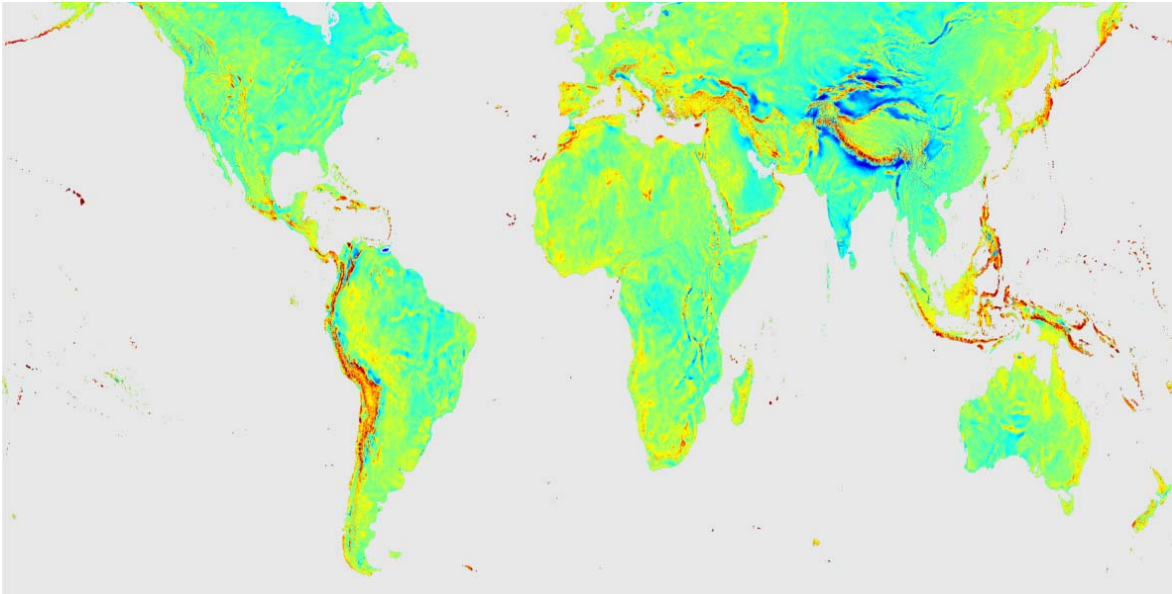
1 General

The development of GGMplus was driven by our vision to provide for the first time widely complete gravity field knowledge on a near-global scale to users of the scientific and engineering community as well as for education purposes based on freely-available data sources.

The model development was facilitated by the availability of new satellite observations of Earth's gravity field, as well as detailed topographic elevation data (Sect. 2), availability of suitable and efficient methods for highest-resolution gravity modelling (Sect. 3) and, importantly, made possible through advanced supercomputing resources provided by the iVEC/Epic supercomputing centre of Western Australia.

Coverage

GGMplus provides computerized gravity field maps at 7.2 arc-seconds (0.002° or ~224 m in latitude direction) resolution for all land areas of Earth within $\pm 60^\circ$ geographic latitude (as represented by SRTM, with the exception of the Southern part of Greenland), and an adjoining ~10 km marine zone along the coast lines (Fig. 1). The target resolution of GGMplus of 7.2 arc-seconds translates into a total of ~3 billion computation points within our working area. The chosen resolution allows representing the short-scale variations of the radial (gravity) and horizontal field components (deflections of the vertical).



402 **Figure 1.** Coverage of GGMplus. Shown are mean values of the radial component of the gravity
 403 field over land and near-coastal areas between $\pm 60^\circ$ geographic latitude.
 404

405
 406 *Technical definitions*

407
 408 The five gravity field functionals provided by GGMplus are

- 409
- 410 • Free-fall gravity accelerations (i.e. gravitational plus centrifugal accelerations)
 - 411 • Gravity disturbances (radial derivatives of the disturbing potential), denoted as radial
 412 component of the gravity field in the manuscript
 - 413 • North-South deflection of the vertical in Helmert definition (latitudinal derivative of the
 414 disturbing potential), denoted as horizontal component of the gravity field in the
 415 manuscript
 - 416 • East-West deflection of the vertical in Helmert definition (longitudinal derivative of the
 417 disturbing potential), denoted as horizontal component of the gravity field in the
 418 manuscript
 - 419 • and Molodenski quasigeoid heights.

420
 421 All quantities are given at the Earth's surface as defined through the SRTM (Shuttle Radar
 422 Topography Mission) topography. Users wishing to use geoid heights instead of quasigeoid
 423 heights can do so by applying standard conversion as described, e.g., *Rapp* [1997].

424
 425 **2 Data sets used**

426
 427 A complete list of data sets used for the development of GGMplus is given in Table 1. The use of
 428 these data is further detailed in Section 3.

429
 430 Table 1. Data sets used for the development of GGMplus

Dataset	Ressource	Citation
---------	-----------	----------

GRACE satellite gravity model ITG2010s	http://icgem.gfz-potsdam.de/ICGEM	<i>Mayer-Gürr et al.</i> [2010]
GOCE-TIM4 satellite gravity model	http://icgem.gfz-potsdam.de/ICGEM/	<i>Pail et al.</i> , [2011]
EGM2008 gravity model	http://earth-info.nga.mil/GandG/wgs84/gravitymod/egm2008/	<i>Pavlis et al.</i> , [2012]
Gridded 250 m SRTM V4.1 release over land	http://srtm.csi.cgiar.org/	<i>Jarvis et al.</i> , [2008]
Gridded SRTM30_PLUS V7 bathymetry offshore	http://topex.ucsd.edu/WWW_html/srtm30_plus.html	<i>Becker et al.</i> , [2009]
RET2012 spherical harmonic rock-equivalent topography model	http://www.geodesy.curtin.edu.au/research/models, file Earth2012.RET2012.SHCto2160.zip	<i>Hirt et al.</i> , [2012]
Earth2012 Topo/Air spherical harmonic model of Earth's physical surface	http://www.geodesy.curtin.edu.au/research/models, file Earth2012.topo_air.SHCto2160.zip	<i>Hirt et al.</i> , [2012]

431

432 3 Methods

433

434 GGMplus is constructed as a composite model of GOCE and GRACE satellite gravity,
435 EGM2008 and topographic gravity in the space domain. The following steps were taken to
436 develop the model:

- 437 • Combination of GOCE and GRACE satellite gravity (Sect. 3.1)
- 438 • Combination of GOCE-GRACE combined model with EGM2008 (Sect. 3.2)
- 439 • Spherical harmonic synthesis of gravity field quantities (Sect. 3.3)
- 440 • Forward-modelling of gravity field quantities (Sect. 3.4)
- 441 • Calculation of normal gravity at the Earth's surface (Sect. 3.5)
- 442 • Combination of synthesis and forward-modelling results (Sect. 3.6)

443

444 The 250 m resolution SRTM topography [*Jarvis et al.*, 2008] is consistently used to represent
445 Earth's physical surface in the gravity field synthesis (Sect. 3.3), forward-modelling (Sect. 3.4)
446 and calculation of normal gravity (Sect. 3.4). In approximation, SRTM elevations are physical
447 heights above mean sea level. In processing steps 3.3 and 3.5, heights of the topography above
448 the ellipsoid (ellipsoidal heights) are required. These were obtained in approximation as sum of
449 SRTM and the EGM2008 quasigeoid [*Pavlis et al.*, 2012]. The geoid-quasigeoid separation was
450 not accounted for in the construction of SRTM ellipsoidal heights, because this effect is mostly
451 small (cm-dm-level, up to 1-2 m in the high mountains), which play a negligible role in 3D
452 spherical harmonic synthesis. The parameters of the GRS80 geodetic reference system [*Moritz,*
453 2000] were consistently used throughout the GGMplus model development.

454

455 3.1 *GOCE TIM4 and GRACE combination*

456

457 The satellite-only combination model has been computed by addition of full normal equations of
458 GRACE and GOCE.

459

460

$$\begin{aligned}
 & \left[\sum_{i=1}^4 (A^T \Sigma(l)^{-1} A)_{GOCE,i} + A^T \Sigma(l)^{-1} A \right]_{GRACE} x = \\
 & \left[\sum_{i=1}^4 (A^T \Sigma(l)^{-1} l)_{GOCE,i} + A^T \Sigma(l)^{-1} l \right]_{GRACE} \Leftrightarrow N_{sat} x = n_{sat}
 \end{aligned} \tag{1}$$

462

463

464 The GRACE component consists of ITG-Grace2010s [Mayer-Gürr *et al.*, 2010] up to
465 degree/order 180, which is based on GRACE K-band range rate and kinematic orbit data
466 covering the time span from August 2002 to August 2009. The GOCE component contains
467 reprocessed satellite gravity gradiometry data (main diagonal components V_{xx} , V_{yy} and V_{zz} and
468 off-diagonal component V_{xz} of the gravity gradient tensor; summation $i = 1, \dots, 4$ in Eq. (1)) from
469 November 2009 to June 2012, as they have also been used for the 4th release of the GOCE TIM
470 model [Pail *et al.*, 2011]. In Eq. (1), l are the observations, and x the unknown spherical
471 harmonic coefficients (SHC).

472

473 In the frame of the gravity gradient reprocessing, among others an improved algorithm for
474 angular rate reconstruction has been applied [Stummer *et al.*, 2011], leading to a significant
475 improvement of the gravity gradient performance mainly in the low to medium degrees [Pail *et al.*, 2013].
476 The resulting GOCE gradiometry normal equations are resolved up to degree/order
477 250.

478

479 Special emphasis has been given to realistic stochastic modeling of observation errors as part of
480 the assembling and solution of the individual normal equation systems, yielding realistic
481 variance-covariance information $\Sigma(l)$ for both GRACE and GOCE. In the case of GOCE, digital
482 auto-regressive moving average (ARMA) filters have been used to set-up the variance-
483 covariance information of the gradient observations [Pail *et al.*, 2011]. Technically, this is done
484 by applying these filters to the full observation equation, i.e., both to the observations and the
485 columns of the Jacobian (design matrix A). Due to the realistic stochastic modeling, the two
486 normal equations could be combined with unit weight. Because of the further combination with
487 EGM2008 as described in section 3.2, regularization has not been applied.

488

489 3.2 *GOCE/GRACE and EGM2008 combination*

490

491 The combination of the GRACE/GOCE data with EGM2008 is done on the basis of the
492 combined GRACE/GOCE normal equations (see Sect. 3.1). Here the EGM2008 SHCs are
493 treated as a set of *a priori* known parameters introduced into a least-squares process of the form:

494

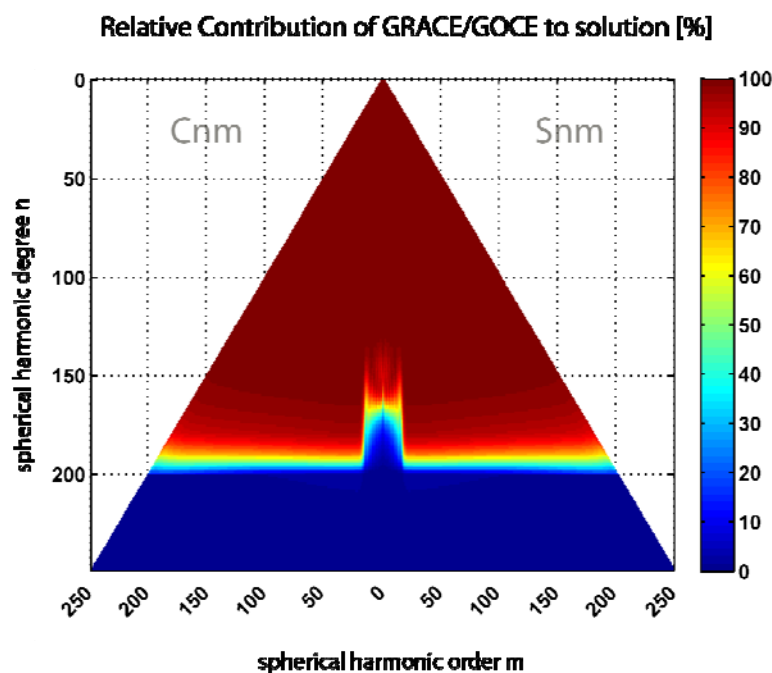
$$(w_1 N_{sat} + w_2 \Sigma(x_{EGM})^{-1}) x = w_1 n_{sat} + w_2 \Sigma(x_{EGM})^{-1} x_{EGM} \tag{2}$$

496

497 where x is the optimally combined set of SHCs from GRACE, GOCE and EGM2008. The
 498 terms N_{sat} and n_{sat} denote the normal equation system of GRACE/GOCE combination (cf.
 499 section 3.1), resolved up to degree/order 250.

500
 501 The terms $\Sigma(x_{EGM})^{-1}$ and $\Sigma(x_{EGM})^{-1}x_{EGM}$ denote the system of normal equations, which relies
 502 exclusively on the EGM2008 coefficients x_{EGM} up to degree/order 360, which are used as
 503 pseudo-observations (the Jacobian is in this case an identity matrix). Since for EGM2008 only
 504 the variances are available, the variance-covariance matrix $\Sigma(x_{EGM})^{-1}$ has a diagonal structure.
 505 The weight for the satellite-only system is $w_1 = 1$, expressing the fact that we consider the formal
 506 errors of this combined model as correctly scaled, and the weight of EGM2008 has been
 507 assigned empirically with $w_2 = 0.16$, and the EGM2008 formal errors have been down-scaled by
 508 a factor of 1 increasing linearly to 10 in range of degrees 180 to 200. In this way, the
 509 combination is tuned giving GRACE/GOCE data dominant influence in the degrees 0 to 180 and
 510 forcing EGM2008 information to take over in the spectral range 200 to 2190, leaving the main
 511 spectral range of transition from GRACE/GOCE to EGM2008, where both components
 512 contribute significantly, between degrees 180 to 200. Figure 2 shows the relative contributions of
 513 GOCE/GRACE data (red for more than 80% GOCE/GRACE impact) and indirectly the
 514 EGM2008 model contribution (blue for more than 80% EGM2008 impact) per spherical
 515 harmonic coefficient C_{nm} / S_{nm} in the combination (for degrees 0 to 250).

516

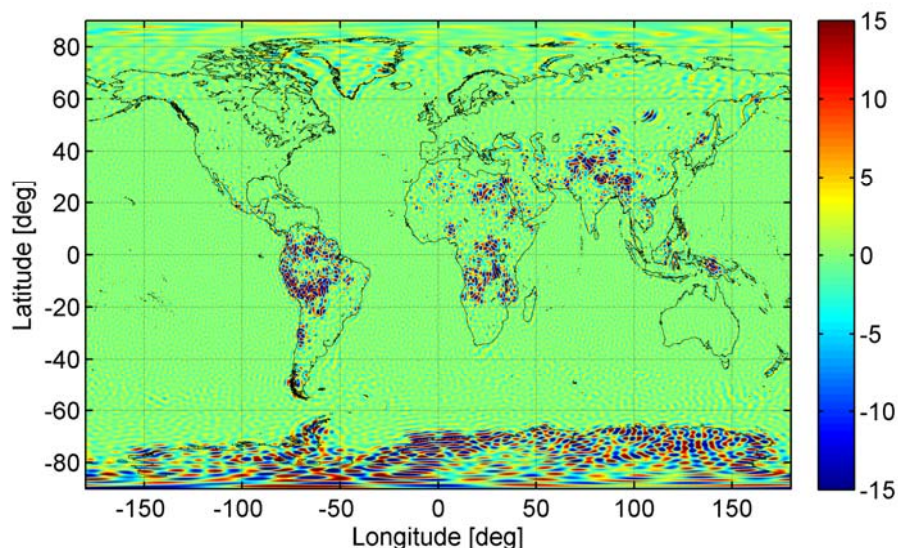


517
 518 Figure 2. Relative contribution of GOCE/GRACE data per spherical harmonic coefficient
 519 C_{nm} / S_{nm} in the combination with EGM2008 data (in percent) for the degrees 0 to 250

520
 521 From Fig. 2, the transition for certain harmonic orders (say $-20 < m < +20$) is differently than the
 522 other orders (say $m < -20$, $m > +20$). This is related to the lower accuracy for the determination of

523 the near-zonal spherical harmonic coefficients using GOCE gradiometry (known as the polar gap
524 problem due to the GOCE satellite's orbit inclination of 96.6 degrees). The lack of observations in
525 the polar regions worsens the accuracy in the determination of a certain group of spherical
526 harmonic coefficients, which is the near-zonal group (e.g., Sneeuw and Gelderen, 1997).
527 Consequently in the combined solution EGM2008 has a higher influence in for those coefficients
528 where GOCE shows a lower performance (and thus a higher standard deviation).
529

530 The outcome of this processing step is a combined GRACE/GOCE/EGM2008 coefficient data
531 set here denoted as GGE. Figure 3 shows the differences between gravity disturbances from
532 GGE and EGM2008, revealing significant discrepancies at the 10-20 mGal-level over Africa,
533 Asia and South America, while there is agreement in the mGal range over most parts of Europe,
534 Australia and North-America. The larger discrepancies are interpreted as improvements over
535 EGM2008 conferred by recent GRACE and GOCE data to GGMplus, see also *Pail et al.*, [2011]
536 and *Hirt et al.*, [2012].
537



538
539 Figure 3. Gravity disturbance differences between the GRACE/GOCE/EGM2008 merger GGE
540 and EGM2008-only in the spectral band of degrees 2 to 250, units in mGal
541

542 3.3 Synthesis

543
544 The spherical-harmonic coefficients (SHCs) of the combined GGE model were used in the
545 spectral band of degrees 2 to 2190 to synthesize gravity field functionals at the Earth's surface,
546 as represented through the 3D-coordinates (latitude, longitude, height). Accurate evaluation of
547 the SHCs requires taking into account the ellipsoidal height of the evaluation points which were
548 obtained from SRTM at 7.2 arc-second resolution. The zonal harmonics of the GRS80 normal
549 gravity field were subtracted from the GGE-model SHCs as described in *Smith* [1998]. The tide
550 system used in the synthesis is zero-tide, which is compatible with GRS80 [*Moritz*, 2000].
551

552 Spherical harmonic synthesis of gravity field functionals at the Earth's surface – known as 3D
553 synthesis – is computationally extraordinarily demanding, because efficient SHS operations

554 cannot be used [Holmes, 2003]. Therefore we used the gradient approach to higher order [Hirt,
 555 2012] which offers an efficient yet accurate approximate solution for 3D synthesis at densely-
 556 spaced surface points, represented through the elevation model. We used a modification of the
 557 harmonic_synth software [Holmes and Pavlis, 2008] to synthesize quasigeoid heights, gravity
 558 disturbances, North-South and East-West deflections of the vertical at a reference height of 4 km
 559 above the GRS80 reference ellipsoid at 1 arc-min resolution. For all four functionals radial
 560 derivatives were computed up to 5th-order at the same reference height and resolution. These
 561 were bicubically interpolated to 7.2 arc-second resolution and continued from the reference
 562 height to the Earth's surface with 5th-order Taylor series expansions (cf. generic formulations
 563 provided in Hirt [2012]), yielding numerical estimates of gravity functionals at 3 billion surface
 564 points in the spectral band of degrees 2 to 2190.

565
 566 Using the gradient approach as described, the 3D synthesis of the four gravity field functionals
 567 took about 6 weeks of computation time using an in-house Sun Ultra 45 workstation. By
 568 comparison, 3D synthesis with conventional point-by-point evaluation methods [Holmes, 2003]
 569 would have taken an estimated 60 years of computation time. This estimate is based on an
 570 observed performance of 100 points/ minute using the same workstation and parameters. The 3D
 571 synthesis as applied here is therefore one of the key innovations that made the construction of
 572 GGMplus feasible within acceptable computation times.

573
 574 We note that the gradient approach is an approximate technique for 3D-SHS, whereby
 575 approximation errors decrease with increasing order of the Taylor series applied. From analysis
 576 of the 0th to 5th-order contributions over 3 billion points, the contribution made by subsequent
 577 orders (e.g., 0th and 1st, 1st and 2nd) differs by a factor of about 4 to 5 (see also Table 2). Given
 578 maximum contributions of 2 mm, 0.6 mGal and 0.1 arc-sec for the 5th-order, maximum
 579 approximation errors (due to truncation of the Taylor series after the 5th-order) will be generally
 580 smaller than 0.6 mm, 0.2 mGal and 0.03 arc-sec anywhere in our working area. Hence, the
 581 Taylor series as applied for GGMplus converge sufficiently, and approximation errors are
 582 negligible for practical applications.

583
 584 Table 2. RMS (root-mean-square) and maximum values of the 4th-order and 5th-order terms of
 585 the Taylor expansions used for gravity field continuation to the Earth's surface. Also given are
 586 the estimated RMS and maximum approximation errors. Values reported for the functionals
 587 quasigeoid, gravity disturbances and deflections of the vertical.

Functional	Contribution of 4 th -order term		Contribution of 5 th -order term		Estimated approximation error	
	RMS	Max	RMS	Max	RMS	Max
Quasigeoid [mm]	0.24	9.88	0.05	2.07	0.01	0.52
Gravity [mGal]	0.06	2.54	0.01	0.59	0.00	0.15
NS deflection of the vertical [arc-sec]	0.01	0.31	0.00	0.08	0.00	0.02
EW deflection of the vertical [arc-sec]	0.01	0.34	0.00	0.08	0.00	0.02

588
 589 For quasigeoid heights, the C1B correction term [Rapp, 1997], see also [Hirt, 2012], was applied
 590 to take into account the change in normal gravity with height. For gravity disturbances, the

591 ellipsoidal correction was applied [Claessens, 2006]. For the North-South deflection of the
592 vertical, corrections for the curvature of the plumbline and for the ellipsoidal effect were taken
593 into account as described in [Jekeli, 1999].

594

595

596 3.4. Forward-modelling

597

598 Gravity forward-modelling based on high-resolution topography is a frequently-used technique
599 to derive information on the short-scale gravity field in approximation [Forsberg, 1984; Pavlis et
600 al., 2007; Hirt, 2012]. The short-scale (i.e., 10 km to ~250 m) gravity signals of the GGMplus
601 model are based on forward-modelling using the 7.5 arc-sec resolution (~250m) SRTM V4.1
602 topography [Jarvis et al., 2008] over land and the 30 arc-sec resolution SRTM30_PLUS V7.0
603 bathymetry [Becker et al., 2009] over sea. A small number of bad data areas (about 0.002% of
604 the total area covered by GGMplus as shown in Fig. 1) was identified and removed from both
605 data sets through simple hole-filling.

606

607 The forward-modelling approach applied here follows the description given in Hirt [2013]. In
608 brief, we converted the SRTM30_plus bathymetry to rock-equivalent depths before merging with
609 the 250m SRTM V4.1 topography. The merger was high-pass filtered by subtracting heights
610 from the RET2012 rock-equivalent topography model to degree and order 2160 (publicly
611 available from <http://geodesy.curtin.edu.au/research/models/Earth2012/>,
612 Earth2012.RET2012.SHCto2160.dat).

613

614 We applied brute-force numerical integration techniques [Forsberg, 1984] to convert the high-
615 pass filtered topography (and rock-equivalent depths over sea) to topography-implied gravity,
616 geoid and vertical deflections. The forward-modelled gravity signals possess spectral energy at
617 spatial scales of ~10 km to ~250 m which augments GGE gravity information beyond 10 km
618 resolution. The numerical integration was accomplished with a variant of the TC software
619 [Forsberg, 1984] and an integration cap radius of 200 km around any of the ~3 billion
620 computation points, and the correction for Earth's curvature applied, as described in Forsberg
621 [1984]. Given the oscillating nature of the high-pass filtered topography, the effect of remote
622 masses largely cancels out as pointed out by Forsberg and Tscherning [1981]. The integration
623 radius chosen is suitable for forward-modelling of high-frequency gravity effects [Hirt et al.,
624 2010; Hirt, 2012].

625

626 The forward-modelling exercise was partitioned into ~19,000 computationally 'manageable'
627 areas of 1 deg x 1 deg extension covering land areas everywhere on Earth between $\pm 60^\circ$ -latitude
628 with SRTM data available. Each 1 deg x 1 deg tile is composed of 625,000 computation points at
629 7.2 arc-seconds resolution. We utilized the iVEC/Epic supercomputing facility
630 (<http://www.ivec.org/>) along with massive parallelization (simultaneous use of up to 1100 central
631 processing units (CPUs)) to accomplish the forward-modelling for the first time near-globally.
632 Based on non-parallelized standard computation techniques and a single CPU, the calculation of
633 topographic gravity effects had taken an estimated 20 years, which is why all previous efforts
634 were inevitably restricted to regional areas.

635

636 The topographic gravity effects calculations are based on the assumptions of constant mass-
637 density (standard rock density 2670 kg/m^3) and isostatically uncompensated topography, which
638 should well be justified given the spatial scales (less than 10 km) modelled here from
639 topographic information (e.g., *Torge*, [2001]; *Watts*, [2001]; *Wieczorek*, [2007]). Given that any
640 gravity field signals originating from mass-density variations [with respect to standard rock
641 density] are not represented by the topographic gravity, our GGMplus gravity maps cannot
642 provide geological information at scales less than 10 km. However, the same limitations apply to
643 EGM2008 at spatial scales less than ~ 27 km over many developing countries [*Pavlis et al.*,
644 2012] and to any other gravity field model with topographic information used to increase the
645 resolution among observed gravity.

646

647 Due to the chosen constant mass-density - often used as standard mass-density for gravity
648 reductions in geophysics and geodesy - the chosen value should approximates well the
649 topographically-induced gravitational attraction over granite rock (2700 kg m^{-3}), while the
650 approximation may introduce errors up to 7% over areas of volcanic rock (2900 kg m^{-3}), and
651 about ~ 26 % where sediments prevail (2000 kg m^{-3}). While inclusion of detailed mass-density
652 maps in the forward-modelling can reduce these errors, a detailed modelling of mass-density
653 variations was not attempted in this work because high-resolution density maps were not
654 available everywhere in our working area.

655

656 From comparisons with ground-truth data sets, a range of studies [e.g., *Hirt et al.*, 2010; *Hirt*,
657 2012; *Šprlák et al.*, 2012] demonstrate that short-scale topographic gravity effects are capable of
658 representing a significant portion (in some cases as high as 90 %) of real gravity field features
659 over rugged terrain, see also evaluation results in Section 5.

660

661 *3.5 Calculation of normal gravity at the Earth's surface*

662

663 For the construction of gravity acceleration maps, normal gravity (i.e., the gravitational attraction
664 and centrifugal acceleration generated by an oblate equipotential ellipsoid of revolution) was
665 calculated at the Earth's surface. We used the parameters of the GRS80 reference ellipsoid
666 [*Moritz*, 2000] along with the standard second-order Taylor expansion (*Torge* [2001], p 110, Eq.
667 4.63) to calculate normal gravity at the ellipsoidal heights of the Earth's surface, as represented
668 through the SRTM topography at 7.2 arc-sec spatial resolution. Beside the gravitational
669 attraction and centrifugal acceleration of the GRS80 mass-ellipsoid, the resulting normal gravity
670 values also contain the effect of gravity attenuation with height (free-air effect), because we
671 evaluated at the Earth's surface.

672

673 *3.6 Combination of synthesis results, forward-modelling and normal gravity*

674

675 All GGMplus gravity field functionals (quasigeoid heights, gravity disturbances, vertical
676 deflections) are the sum of

- 677 • Synthesized functionals from the GGE SHCs (providing the spatial scales of ~ 10000 km
678 down to ~ 10 km, Sect. 3.3) and
- 679 • Forward-modelled functionals from high-pass filtered topography/bathymetry data
680 (providing the spatial scales from ~ 10 km down to ~ 250 m, Sect. 3.4).

681 GGMplus gravity accelerations were obtained as the sum of GGMplus gravity disturbances and
 682 normal gravity values (Sect 3.5).

683

684 **4 Gravity estimation outside working area**

685

686 Due to Earth’s flattening, obvious candidate locations for Earth’s maximum gravity acceleration
 687 are expected near the poles, which is outside the $\pm 60^\circ$ -SRTM latitude band. To include a likely
 688 location for Earth’s maximum gravity acceleration in our work, we obtained gravity
 689 accelerations globally at 5-arc-min resolution without short-scale topographic gravity estimates,
 690 as follows:

- 691 1 We constructed a 5-arcmin grid of approximate ellipsoidal heights of the Earth’s surface
 692 as the sum of elevations from the Earth2012 Topo/Air model (representing Earth’s
 693 physical surface as lower interface of the atmosphere above mean sea level) and the
 694 EGM2008 quasigeoid applied as a correction.
- 695 2 We applied the gradient approach for harmonic synthesis (Sect. 3.3) to fifth-order,
 696 yielding gravity disturbances at the Earth’s surface in spectral band 2 to 2190 using the
 697 GGE coefficients (Sect 3.1).
- 698 3 We calculated normal gravity at the ellipsoidal heights of the Earth’s surface as described
 699 in Sect 3.5) and added the gravity disturbances, yielding gravity accelerations at 5 arc-
 700 min resolutions.

701 Steps 1 and 2 were applied to calculate a global 5 x 5 arc-min grid of quasigeoid heights which
 702 was then used to locate where the quasigeoid is likely to be furthest below the ellipsoid. The
 703 locations of the minimum and maximum gravity accelerations and quasigeoid heights are
 704 reported in Tables S3 and S4.

705

706 **Table 3. Extreme values of gravity accelerations estimated based on 5 arc-min resolution**

Extreme value	Latitude	Longitude	Value [mGal]	Comment
Minimum gravity acceleration	-9.88	-77.21	976790	GGMplus suggests a smaller value at a nearby location.
Maximum gravity acceleration	86.71	61.29	983366	Located offshore in the Arctic sea, not covered by GGMplus. Location and value reported in Table 1 in the main paper.

707

708 **Table 4. Extreme values of quasigeoid heights estimated based on 5 arc-min resolution**

Extreme value	Latitude	Longitude	Value [m]	Comment
Minimum quasigeoid height	4.71	78.79	-106.59	Located offshore (Laccadive Sea, South of Sri Lanka), not covered by GGMplus. Location and value reported in Table 1 in the main paper.
Maximum quasigeoid height	-4.21	138.71	86.48	GGMplus suggests a larger value at another location.

709

710 **5. Model evaluation**

711

712 We have evaluated GGMplus gravity field functionals using (i) gravity accelerations from
 713 terrestrial gravimetry, (ii) deflections of the vertical from geodetic-astronomical observations,
 714 and (iii) observed quasigeoid heights from GPS ellipsoidal heights and geodetic levelling
 715 (GPS/levelling). The data sets used are summarized in Table 5. Each set of observations is
 716 compared against the three modelling variants

717

- 718 • satellite-only gravity (GRACE combined with 4th-GOCE release) to degree and order 200
 719 (resolution of ~100 km)
- 720 • satellite gravity combined with EGM2008 (GGE), to degree 2190 (resolution of ~10 km)
- 721 • GGMplus (resolution of ~200 m)

722

723 The descriptive statistics of the differences “observation minus model” are reported in Tables 6
 724 and 7 for gravity disturbances, in Table 8 for deflections of the vertical and in Table 9 for
 725 quasigeoid heights. From the comparisons over North America, Europe and Australia – areas
 726 with good ground gravity coverage – the accuracy of GGMplus is at the 3-5 mGal, 1 arc-sec and
 727 5-7 cm level or somewhat better for gravity, deflections of the vertical and quasigeoid heights,
 728 respectively. The RMS-improvements conferred by the short-scale gravity modelling (compare
 729 GGMplus with GGE) range between ~20 to ~90 % for the radial (gravity) and horizontal field
 730 components (deflections of the vertical), and is lower (non-significant to ~40% over Switzerland
 731 as an example of a mountainous region) for quasigeoid heights. Fig. 4 exemplifies the good
 732 agreement between observed gravity and GGMplus over Australia. The differences mostly
 733 reflect the effect of local mass-density variations, and can be used for geophysical interpretation.
 734 Fig. 4 also shows oscillations of 1-2 mGal amplitude and ~200 km full-wavelength which are
 735 likely to reflect the error level of GOCE satellite observations used in GGMplus.

736

737 Over less well-surveyed areas, the differences increase to ~8 to ~23 mGal, as is indicated by the
 738 few ground gravity observations available. Given that the forward-modelling of gravity effects at
 739 spatial scales of ~10 km to 200 m is based on a homogeneous procedure everywhere between ±
 740 60° geographic latitude, there is no reason to assume a reduced performance over Asia, Africa
 741 and South America. The deterioration rather reflects the limited data availability for EGM2008 at
 742 spatial scales of ~100 to 10 km. The accuracy of GGMplus gravity field functionals is therefore
 743 largely dependent on the EGM2008 model commission errors, which can be as high as ~30-35
 744 cm for quasigeoid heights, and ~4 arc-seconds for deflections of the vertical [Pavlis *et al.*, 2012].
 745 We therefore expect the GGMplus accuracy to deteriorate by factor 3-5 from well-surveyed to
 746 poorly-surveyed continents.

747

748 Table 5. Gravity field observations used for evaluation of GGMplus.

Observation type	Country/ Area	# Stations	Data source/provider
Gravity accelerations and disturbances from terrestrial	United States	1,277,637	University of Texas at el Paso http://research.utep.edu/default.aspx?tabid=37229 2012 release
	Australia	1,625,018	Geoscience Australia

gravimetry			http://www.geoscience.gov.au 2013 release
	Switzerland	31,598	Swisstopo, Dr U Marti
	Central Africa	41,148	Bureau Gravimétrique International, Dr S Bonvalot
	India/Himalayas	7,562	Bureau Gravimétrique International, Dr S Bonvalot
	Northern South-America	12,150	Bureau Gravimétrique International, Dr S Bonvalot
Deflections of the vertical from geodetic- astronomical observations	United States	3,396	National Geodetic Survey, Drs D Smith and Y Wang
	Australia	1,063	Geoscience Australia/ Dr W Featherstone (Curtin University)
	Europe	1,056	ETZ Zurich, Dr B Bürki; Swisstopo, Dr U Marti; first author's own observations
GPS/levelling/ quasigeoid heights	United States	18972	National Geodetic Survey, http://www.ngs.noaa.gov/NGSDataExplorer/
	Germany	675	Bundesamt für Kartographie und Geodäsie, U Schirmer
	Switzerland	193	Swisstopo, Dr U Marti

749

750

Table 6. Descriptive statistics of the differences observed gravity minus models, units in mGal

Terrestrial data	Model	Min	Max	Mean	RMS
US gravity	Satellite-only	-238.85	204.19	6.83	27.41
	GGE	-271.88	110.10	-2.70	10.80
	GGMplus	-303.39	88.84	-0.68	3.49
Australian gravity	Satellite-only	-179.98	118.24	-1.14	14.88
	GGE	-194.33	82.65	-1.07	5.03
	GGMplus	-193.15	81.06	-0.71	2.90
Swiss gravity	Satellite-only	-235.04	131.13	-35.49	67.21
	GGE	-226.64	93.38	-17.59	39.72
	GGMplus	-91.23	28.71	-0.60	4.41

751

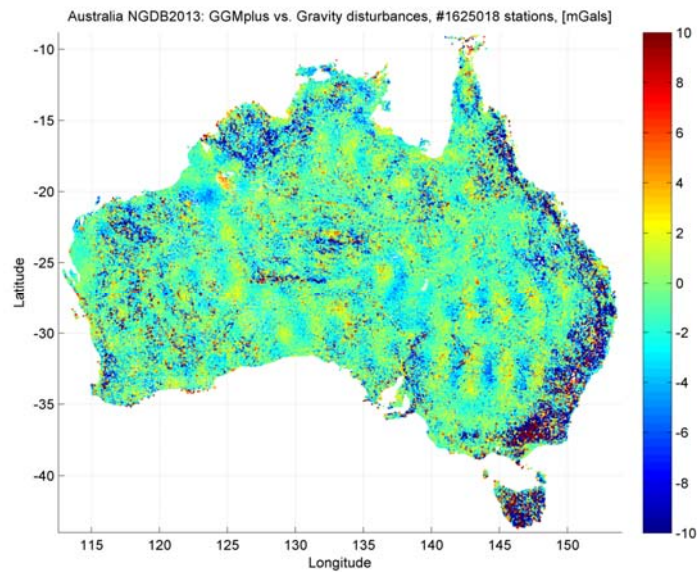
752

Table 7. Descriptive statistics of the differences observed gravity minus models, units in mGal

Terrestrial data	Model	Min	Max	Mean	RMS
Central Africa	Satellite-only	228.79	394.56	- 1.33	26.91
	GGE	-275.02	403.27	-0.15	9.68
	GGMplus	-284.41	399.87	0.37	8.24
India+ Himalayas	Satellite-only	-329.51	365.47	-5.23	43.53
	GGE	-184.46	341.92	0.04	21.84
	GGMplus	-182.44	309.74	2.45	13.76
Northern South- America	Satellite-only	-247.71	365.75	-11.66	66.52
	GGE	-224.32	361.48	-4.60	26.18
	GGMplus	-234.27	364.00	-0.03	22.69

753

754



755

756 Figure 4. Differences between observed gravity accelerations and GGMplus over Australia, units
 757 in mGal.

758

759 Table 8. Descriptive statistics of the differences observed deflection of the vertical (DoV) minus
 760 models, units in arc-seconds

Terrestrial data	Model	Min	Max	Mean	RMS
US North-South DoVs	Satellite-only	-19.59	22.62	0.20	3.27
	GGE	-12.55	21.29	0.09	1.11
	GGMplus	-12.58	20.97	-0.02	0.84
US East-West DoVs	Satellite-only	-22.66	23.41	0.29	3.78
	GGE	-13.57	12.38	0.10	1.14
	GGMplus	-6.19	9.90	0.12	0.78
Australian North-South DoVs	Satellite-only	-11.58	11.76	-0.14	2.21
	GGE	-5.00	3.44	-0.23	0.81
	GGMplus	-5.13	2.61	-0.19	0.66
Australian East-West DoVs	Satellite-only	-18.01	11.68	-0.14	2.63
	GGE	-4.87	3.60	-0.11	1.04
	GGMplus	-5.05	4.05	-0.13	0.97
Europe North-South DoVs	Satellite-only	-19.49	26.96	0.88	6.41
	GGE	-15.06	15.62	0.05	3.02
	GGMplus	-4.86	5.51	-0.05	1.06
Europe East-West DoVs	Satellite-only	-24.05	24.97	0.90	5.87
	GGE	-11.58	15.65	0.38	2.98
	GGMplus	-4.29	4.99	0.23	1.09

761

762

763

764

765 Table 9. Descriptive statistics of the differences observed quasigeoid height minus models, units
 766 in m. In case of US GPS/levelling data, observed geoid heights were converted to quasigeoid
 767 heights applying Rapp's (1997) formalism [1] prior to comparison with the three modelling
 768 variants. A bias (Germany, Switzerland), and tilted plane (US) were subtracted.

Terrestrial data	Model	Min	Max	RMS
US GPS/lev	Satellite-only	1.80	2.72	0.367
	GGE	-0.34	0.42	0.070
	GGMplus	-0.36	0.43	0.070
German GPS/lev	Satellite-only	-1.07	1.42	0.315
	GGE	-0.11	0.17	0.042
	GGMplus	-0.10	0.14	0.041
Swiss GPS/lev	Satellite-only	-1.27	1.86	0.605
	GGE	-0.24	0.18	0.076
	GGMplus	-0.17	0.13	0.046

769

770 Additional References

771

772 Becker, J.J., D.T. Sandwell, W.H.F. Smith, J. Braud, B. Binder, J. Depner, D. Fabre, J. Factor, S. Ingalls,
 773 S-H. Kim, R. Ladner, K. Marks, S. Nelson, A. Pharaoh, R. Trimmer, J. Von Rosenberg, G. Wallace
 774 and P. Weatherall (2009), Global Bathymetry and Elevation Data at 30 Arc Seconds Resolution:
 775 SRTM30_PLUS, *Marine Geod.*, 32(4), 355-371.

776 Claessens, S.J., (2006), Solutions to Ellipsoidal Boundary Value Problems for Gravity Field Modelling,
 777 PhD thesis, Department of Spatial Sciences, Curtin University of Technology, Perth, Australia.

778 Claessens, S.J., W.E. Featherstone, I.M. Anjasmara, and M.S. Filmer (2009), Is Australian data really
 779 validating EGM2008 or is EGM2008 just in/validating Australian data, in *Newton's Bulletin* 4, 207-
 780 251, Publication of the International Association of Geodesy and International Gravity Field
 781 Service.

782 Forsberg, R. (1984), A study of terrain reductions, density anomalies and geophysical inversion methods
 783 in gravity field modelling, Report 355, *Department of Geodetic Science and Surveying*, Ohio State
 784 University, Columbus.

785 Hirt, C. (2012), Efficient and accurate high-degree spherical harmonic synthesis of gravity field
 786 functionals at the Earth's surface using the gradient approach, *J. Geod.*, 86(9), 729-744, doi:
 787 10.1007/s00190-012-0550-y.

788 Hirt, C. (2013), RTM gravity forward-modeling using topography/bathymetry data to improve high-
 789 degree global geopotential models in the coastal zone, *Marine Geod.*, 36(2):1-20,
 790 doi:10.1080/01490419.2013.779334.

791 Hirt C., M. Kuhn, W.E. Featherstone, and F. Goettl (2012), Topographic/isostatic evaluation of new-
 792 generation GOCE gravity field models. *J. Geophys. Res.* B05407.

793 Holmes, S.A., (2003), High degree spherical harmonic synthesis for simulated earth gravity modelling,
 794 PhD Thesis, Department of Spatial Sciences, Curtin University of Technology, Perth, Australia.

795 Holmes S.A., and N.K. Pavlis (2008), Spherical harmonic synthesis software harmonic_synth.
 796 http://earth-info.nga.mil/GandG/wgs84/gravitymod/new_egm/new_egm.html.

797 Jarvis, A., H.I. Reuter, A. Nelson, and E. Guevara. (2008). Hole-filled SRTM for the globe Version 4,
 798 Available from the CGIAR-SXI SRTM 90m database. Available at: <http://srtm.csi.cgiar.org>.

799 Jekeli C (1999), An analysis of vertical deflections derived from high-degree spherical harmonic models.
 800 *J. Geod.* 73(1), 10-22.

801 Mayer-Gürr, T., E. Kurtenbach, and A. Eicker (2010), ITG-Grace2010 Gravity Field Model. URL:
 802 <http://www.igg.uni-bonn.de/apmg/index.php?id=itg-grace2010>, 2010.

803 Moritz, H. (2000), Geodetic Reference System 1980. *J. Geod.*, 74, 128-140.

804 Pail R., T. Fecher, M. Murböck M. Rexer, M. Stetter, T. Gruber, and C. Stummer, (2013), Impact of
805 GOCE Level 1b data reprocessing on GOCE-only and combined gravity field models. *Stud.*
806 *Geophy. Geod.* 57, 155-173.

807 Pavlis, N.K., J.K. Factor, and S.A. Holmes (2007), Terrain-related gravimetric quantities computed for
808 the next EGM, in *Proceedings of the 1st International Symposium of the International Gravity Field*
809 *Service* 318-323, Harita Dergersi, Istanbul.

810 Pavlis N.K., S.A. Holmes, S.C. Kenyon, and J.K. Factor (2012), The development and evaluation of the
811 Earth Gravitational Model 2008 (EGM2008), *J. Geophys. Res.*, 117, B04406,
812 doi:10.1029/2011JB008916.

813 Rapp R.H (1997), Use of potential coefficient models for geoid undulation determinations using a
814 spherical harmonic representation of the height anomaly/geoid undulation difference, *J. Geod.* 71(5),
815 282-289.

816 Smith, D.A. (1998), There is no such thing as "The" EGM96 geoid: Subtle points on the use of a global
817 geopotential model, in *International Geoid Service Bulletin* 8, 17-28, International Geoid Service,
818 Milan, Italy.

819 Sneeuw N., van Gelderen, M. (1997), The polar gap. In: *Geodetic boundary value problems in view of the*
820 *one centimeter geoid. Lecture notes in Earth Sciences*, 65, 559-568, Springer, Berlin,
821 doi:10.1007/BFb0011699

822 Šprlák, M., C. Gerlach, and B.R. Pettersen, (2012), Validation of GOCE global gravity field models using
823 terrestrial gravity data in Norway. *J. Geod. Sci.* 2, 134-143.

824 Stummer C., T. Fecher, and R. Pail (2013), Alternative method for angular rate determination within the
825 GOCE gradiometer processing. *J. Geod.* 85, 585-596 (2011).

826 Torge, W. (2001), *Geodesy, 3rd Edition.*, De Gruyter, Berlin, New York.

827 Watts, A.B. (2001), *Isostasy and Flexure of the Lithosphere.* Cambridge University Press.

828 Wieczorek M.A. (2007), Gravity and topography of the terrestrial planets, in *Treatise on Geophysics* 10,
829 165, Elsevier-Pergamon, Oxford.

830